JOURNAL OF GEOPHYSICAL RESEARCH, VOL. 113, A00C05, doi:10.1029/2008JA013451, 2008

Modeling a force-free flux transfer event probed by multiple Time History of Events and Macroscale Interactions during Substorms (THEMIS) spacecraft

H. Zhang,[1] K. K. Khurana,[1] M. G. Kivelson,[1] V. Angelopoulos,[1] Z. Y. Pu,[2] Q.-G. Zong,[3] J. Liu,[1] and X.-Z. Zhou[1]

Received 3 June 2008; revised 23 August 2008; accepted 16 September 2008; published 16 December 2008.

[1] A flux transfer event (FTE) was encountered by all five Time History of Events and Macroscale Interactions during Substorms (THEMIS) spacecraft just outside the dusk magnetopause on 20 May 2007. In the present paper, we fit the magnetic field observations from multiple satellites to a flux rope model in order to obtain the critical geometric parameters of this FTE. The model used includes both electromagnetic force and pressure gradient force and reduces to a force-free model when the magnetic tension is balanced mainly by the magnetic pressure gradient. The cross-sectional scales of the FTE were estimated to be 0.6×1.3 R_E. The core field direction is found to differ only slightly from the results of the minimum variance analysis and the Grad-Shafranov technique. The maximum electric current density within the FTE was $\sim$100 nA/m^2 and the total current was 0.3 MA, which is comparable with the current per R_E flowing on the local magnetopause. The magnetic flux inside the FTE was $\sim 4 \times 10^5$ Wb. Magnetic field data and plasma data show that this FTE was fully embedded in the boundary region between the magnetosheath and the magnetosphere. The magnetic configuration and the flow distribution around the FTE suggest that X lines were present both ahead of and behind the FTE, but we cannot determine whether these X lines formed synchronously. Our observations favor the conclusion that multiple X line models are the candidate mechanisms for the generation of this FTE, and some of the FTE's features cannot be understood in the frame of any single X line FTE model.

Citation: Zhang, H., K. K. Khurana, M. G. Kivelson, V. Angelopoulos, Z. Y. Pu, Q.-G. Zong, J. Liu, and X.-Z. Zhou (2008), Modeling a force-free flux transfer event probed by multiple Time History of Events and Macroscale Interactions during Substorms (THEMIS) spacecraft, *J. Geophys. Res.*, *113*, A00C05, doi:10.1029/2008JA013451.

1. Introduction

[2] A flux transfer event (FTE) develops when a discrete bundle of newly reconnected magnetic flux is transported along the dayside magnetopause. FTEs were discovered and defined first through observations of transient bipolar perturbations of the magnetic field in the direction normal to the magnetopause [*Russell and Elphic*, 1978]. Although the bipolar signature can also be interpreted as the result of an impulsive penetration into the magnetosphere of solar wind with enhanced pressure [*Lemaire et al.*, 1979; *Sibeck et al.*, 1989; *Sanny et al.*, 1996], it is widely accepted that FTEs are created by magnetic reconnection on the magnetopause, based on the observations of the magnetic field, electric field, plasma and particles [e.g., *Berchem and Russell*, 1984; *Daly et al.*, 1984; *Farrugia et al.*, 1988; *Zong et al.*, 2003; *Wang et al.*, 2006 and *Le et al.*, 2008]. Surveys of the magnetic field data from ISEE by *Berchem and Russell* [1984] and *Rijnbeek et al.* [1984] reveal that FTEs can be observed on both sides of the dayside magnetopause, in the magnetosphere or in the magnetosheath. Most of them occur during the periods of southward interplanetary magnetic field (IMF) but their occurrence rate has been found also to strongly depend on IMF B_{XGSM}, B_{YGSM} but not on the IMF magnitude [*Wang et al.*, 2006]. In these magnetic field topologies antiparallel reconnection [*Crooker*, 1979] or component reconnection [*Gonzalez and Mozer*, 1974; *Cowley*, 1976] can occur on the dayside magnetopause [*Dungey*, 1961]. When the sheath field connects to the geomagnetic field, the connected flux tube forms a channel between the magnetosphere and the solar wind allowing exchange of mass, momentum and energy. The mixture of the tenuous and hot magnetospheric plasma and dense and warm magnetosheath plasma is a common feature of an FTE and confirms the connectivity between the two regions [e.g., *Daly et al.*, 1981; *Paschmann et al.*, 1982 and recently

[1]Institute of Geophysics and Planetary Physics, University of California, Los Angeles, California, USA.
[2]School of Earth and Space Sciences, Peking University, Beijing, China.
[3]Center for Atmospheric Research, University of Massachusetts, Lowell, Massachusetts, USA.

0148-0227/08/2008JA013451$09.00

Pu et al., 2005]. As agents for magnetosphere-solar wind coupling, FTEs have drawn a lot of attention.

[3] Although it is widely accepted that an FTE is a reconnection-related phenomenon, how reconnection generates an FTE remains an unsolved problem. In the literature, several models of the structure and formation mechanism of FTEs have been proposed. When the first FTE was discovered, *Russell and Elphic* [1978] interpreted the bipolar structure as the signature of draping of the surrounding fields around a reconnected flux tube, and attributed the enhancement of the field magnitude to the bundle of magnetic flux in the tube. The flux tube was thought to have been generated by temporally and spatially limited single X line reconnection (also termed as transient and patchy reconnection) with the plasma trapped in the bent tube accelerated by the tension force [*Russell and Elphic*, 1978]. *Paschmann et al.* [1982] pointed out that pressure balance requires that the flux tube itself have a helical magnetic structure to balance its enhanced internal pressure and thus that the twisted pressure-balanced structure was a flux rope.

[4] Another model of an FTE on the magnetopause was suggested by *Lee and Fu* [1985]. In their model, two or more parallel X lines simultaneously form when the sheath field and the magnetospheric field are not strictly antiparallel. The reconnection rates are time-varying, and between these X lines flux ropes form and eventually convect away. The axes of the flux ropes align in a direction between that of the sheath and the magnetospheric field. In this model, a flux rope extends a finite length along its axis. The field lines become complicated at the ends of an FTE and some of them connect to the magnetosphere while others connect to the sheath [*Fu et al.*, 1990]. The plasma inside the flux rope is not significantly accelerated perpendicular to its axis since both of its ends are "fixed" on the magnetopause and the flux rope is an obstacle in the jet flows from the reconnection sites [*Fu et al.*, 1990]. On the basis of a global MHD simulation, *Raeder* [2006] revised the multiple X line model. In his scenario X lines form at different times and an FTE results only when the second X line forms.

[5] *Liu and Hu* [1988] and *Pu et al.* [1990] suggested a vortex-induced reconnection model, instead of a multiple X line model, to explain the formation of the flux rope type of FTE under the action of the sheared flow between the magnetosheath and magnetopause. Here the FTE bulge is a vortex with an associated rolled-up magnetic field. Vortical flow around an FTE has been observed by *Liu et al.* [2008] using Time History of Events and Macroscale Interactions during Substorms (THEMIS) data.

[6] *Scholer* [1988] and *Southwood et al.* [1988] proposed a transient and bursty single X line reconnection model for the origin of FTEs, but in their models the FTEs are not flux ropes. When transient and bursty reconnection takes place, the field and the plasma close to the reconnection site are accelerated to form a bubble-like structure, while the field and the plasma far from the reconnection site remain undisturbed. When a spacecraft grazes the bubble, a bipolar signature is obtained.

[7] In order to improve our understanding of the origin of FTEs and to distinguish among the different generation mechanisms, it is critical to understand their detailed properties including their geometry and internal structure (helical or not), their transport properties, and their relations to and interactions with the ambient field and plasma. Determination of their axial orientations has drawn much attention because it is crucial for establishing the properties and behavior of the structures [e.g., *Elphic et al.*, 1980, *Xiao et al.*, 2004, *Zhou et al.*, 2006]. Minimum variance analysis (MVA) of the magnetic field is a widely used technique for inferring the characteristic direction of magnetic structures or transition layers in plasma [*Sonnerup and Cahill*, 1967]. When MVA is used to establish the axes of an FTE, the procedure is referred to as principal axis analysis (PAA) [e.g., *Elphic et al.*, 1980, *Zong et al.*, 1997]. *Xiao et al.* [2004] pointed out that the orientation of a flux rope cannot be determined by PAA unless the path of a spacecraft relative to the flux rope and the structural properties of the flux rope are already known. FTEs' cross-sectional maps can be established through the Grad-Shafranov (GS) reconstruction technique [*Sonnerup and Guo*, 1996; *Hasegawa et al.*, 2006]. For this technique, determination of the axial orientation is critical to the accuracy of the reconstruction.

[8] Another widely used approach to the interpretation of FTE structure is to fit the observations to a parameterized flux rope model, although a caution has been advised that even an excellent fit of data to a flux rope model does not necessarily prove the actual existence of such a flux rope [*Hasegawa et al.*, 2007]. A number of quantitative models have been proposed; most of them assume that flux ropes have circular cross sections (e.g., a force-free model by *Lundquist* [1950], and a non force-free model by *Elphic and Russell* [1983]), although such simple axial symmetry has not been clearly supported by observations. *Moldwin and Hughes* [1991] noticed this issue and modified the circular model by embedding the flux rope in an external sheared field to generate the asymmetry. *Kivelson and Khurana* [1995] introduced a model of a flux rope embedded within a Harris neutral sheet. In this model (hereafter referred to as KK95), the magnetic structure both inside and outside flux rope (ambient field) can be described self-consistently for a class of external field configurations. The model has been successfully applied to the analysis of flux ropes in the magnetotail.

[9] On 20 May 2007, FTE signatures were recorded by all five THEMIS spacecraft outside the dusk magnetopause, and this event has been studied by *Lui et al.* [2008] and *Sibeck et al.* [2008]. The GS reconstruction technique has been applied to this event [*Lui et al.*, 2008] on the basis of data from only one of the five spacecraft (THEMIS-D). In the present paper, we extend the study of the same event by fitting the magnetic observations to the parameterized flux rope KK95 model using information from all five spacecraft. Provided that the plasma (field) conditions are symmetric (antisymmetric) on two sides of an FTE, the KK95 model self-consistently represents the plasma and field properties both inside and outside the FTE. The model is particularly relevant for this study because some of the THEMIS satellites traversed the FTE while others just passed nearby. By fitting we obtain a cross-sectional map of the flux rope that describes the internal and the ambient field. The satisfactory correlation of the model with the observations suggests that the observed FTE had a helical internal structure, i.e., this FTE was a flux rope. Our

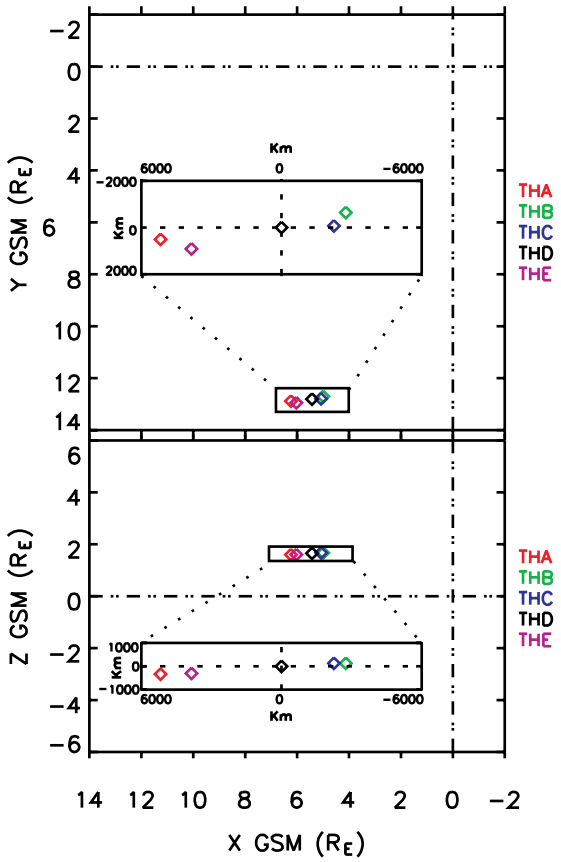

Figure 1. The absolute and relative positions of five THEMIS spacecraft in the GSM coordinate system. The top panel is for the X-Y plane, and the bottom one for the X-Z plane. The absolute positions are illustrated in units of the Earth radius, R_E, while the relative positions are in units of kilometer.

analysis of the plasma flow and the magnetic field geometry leads us to believe that at least two X lines contributed to the formation of the flux rope-type FTE. In the next two sections, we introduce the instrumentation briefly and then display the plasma and magnetic field observations for this event; section 4 gives a detailed description of KK95 model first, and then describes the fitting method and the results of our analysis; our study is discussed and summarized in sections 5 and 6, respectively.

2. Instrumentation

[10] The FTE studied in this paper was recorded by multiple instruments onboard the five THEMIS spacecraft. We have used data from the plasma instruments (the Electrostatic Analyzers (ESA) [*McFadden et al.*, 2008] and the Solid State Telescopes (SST) and the Fluxgate Magnetometers (FGM) [*Auster et al.*, 2008]. The ESA instruments obtain full three-dimensional velocity distributions of both ions and electrons, covering the energy range from ~5 eV to 20 keV, as well as their densities, velocities and temperatures. The hot electrons and ions in the energy range from 25 keV up to 6 MeV are measured by SST instruments. All the moment data presented in this paper are used at 3-s resolution; FGM data at 0.25-s resolution were used for our fit to the magnetic field.

[11] At about 2200 UT on 20 May 2008, when the five THEMIS spacecraft encountered the FTE, they were inbound in a pearls-on-a-string configuration and crossed the duskside magnetopause into the magnetosphere [*Angelopoulos*, 2008]. THEMIS-D (THD) was located at (5.43, 12.81, 1.65) R_E in the GSM coordinate system, and the relative positions of THA, THB, THC and THE with respect to THD were (5182.58, 522.00, −332.91), (−2753.65, −651.38, 127.11), (−2244.28, −77.80, 131.13) and (3859.44, 924.36, −299.36) km in GSM, respectively. The absolute and relative positions of each spacecraft are shown in Figure 1. It is clear that all five spacecraft were approximately colinear and aligned mainly in the X direction. In this configuration, the five THEMIS satellites traversed the FTE and its near surroundings, which made it feasible to collect extensive two-dimensional information regarding the FTE's cross section.

3. Observations

3.1. Magnetic Field Signatures

[12] The determination of the normal to the magnetopause is critical for analyzing an FTE event on the magnetopause [*Russell and Elphic*, 1978]. In the present event, the magnetopause had been disturbed locally by the FTE and it is not easy to determine a unique normal direction. Thus we estimate it from an empirical model [*Shue et al.*, 1998; *Wang et al.*, 2005], and at the location where THEMIS encountered the FTE, the modeled normal to the magnetopause, denoted by $\vec{N}$, was (0.692, 0.715, 0.092) in GSM. We introduce a local magnetopause coordinate system (LMN) with $\vec{N}$ pointing outward along the normal to the magnetopause, $\vec{M}$ along (−0.715, 0.693, 0.000), determined by $\vec{z} \times \vec{N}$, where $\vec{Z}$ denotes the Z axis of the GSM coordinate system, and $\vec{L}$ along (−0.064, −0.066, 0.992) determined by $\vec{N} \times \vec{M}$.

[13] Figure 2 presents an overview of the FGM data of all five spacecraft in the local magnetopause coordinate system (LMN). During the time of interest, the THEMIS spacecraft encountered two regions with different magnetic field characteristics. In both regions, the dominant components were B_L and B_M. The magnetic field was strong and steady in one region and the total field was greater than 30 nT. In the other region the magnetic field was disturbed and weak, with magnitude less than 20 nT. We interpret the two different regions as the magnetosphere and the magnetosheath, respectively. During the time interval of Figure 2, three spacecraft, THB, −C and −D were initially located in the magnetosphere, and later they alternated between the magnetosheath and the magnetosphere. Around 2202 UT, after the three spacecraft reentered the magnetosheath, they encountered a structure with bipolar signals in both B_N and B_M. The magnitude of the perturbation of B_N was clearly larger than its average background level. The enhancements in B_L and B_T at THD were most significant (~50 nT), while they were weaker at THB and THC. These magnetic perturbations are the typical signatures of an FTE near the magnetopause [*Russell and Elphic*, 1978]. Throughout the interval shown in Figure 2 except when the FTE was encountered, the outermost two satellites, THA and THE,

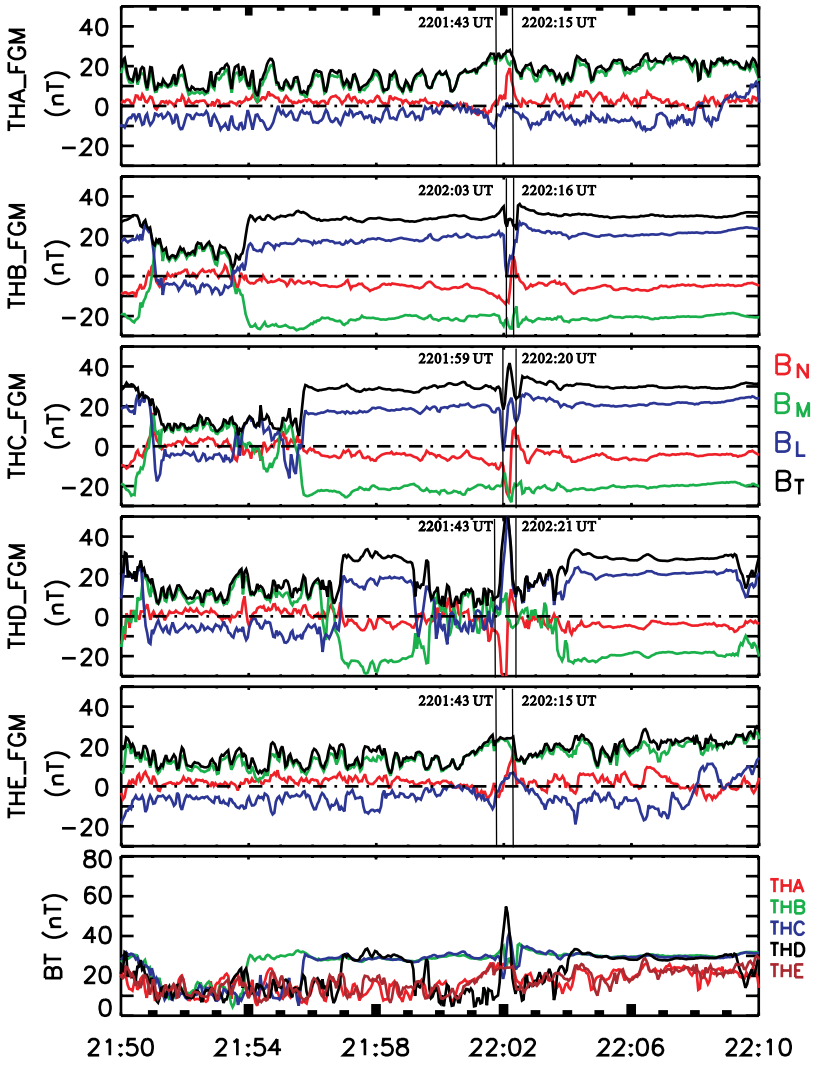

Figure 2. An overview of the FGM data from all five THEMIS spacecraft. FGM data from the five spacecraft of THEMIS are shown in the magnetopause local coordinate system ($\vec{N}$, $\vec{M}$, $\vec{L}$) with $\vec{N}$ along the normal of the magnetopause, $\vec{M}$ determined by $\vec{Z} \times \vec{N}$, where $\vec{Z}$ denotes the Z axis in GSM, and $\vec{L}$ determined by $\vec{N} \times \vec{M}$. The vertical lines in each panel mark the time interval of the FTE signatures. The magnitudes of the magnetic field at all five spacecraft are plotted in the bottom panel for comparison.

were located in the magnetosheath, and their B_N components remained small. When the FTE was encountered by the two spacecraft, there were only positive perturbations but no clear bipolar structures in the B_N component especially at THA, and B_T increased to a value (~25 nT) between the magnitude of the sheath field (less than 20 nT) and the magnetosphere field (~30 nT). The FTE signatures at each spacecraft are marked by vertical lines in Figure 2.

[14] It is worth emphasizing that the peaks of B_T and B_L significantly exceed their values in the nearby magnetosphere and that the perturbations of B_N and B_M are far larger at THD than at the other spacecraft. This supports the view that THD crossed the FTE close to its center. The outermost spacecraft (THA and THE) flew by the FTE on the flank near the magnetosheath, and B_T during the flyby increased to 25 nT; the dominant component was B_M. The innermost two spacecraft, THB and THC grazed or flew by the edge of the FTE closest to the magnetosphere, and between the FTE and the magnetosphere (before and after the FTE) both THB and THC detected dips in B_T with the magnitude of about 25 nT which is similar with those obtained by THA and THE just outside the FTE (see the bottom panel of Figure 2). The difference is that in these dips the dominant component, B_M, is the negative, whereas at THA and THE the B_M component was positive. The magnitude dips indicate that

Figure 3. The plasma observations from THD. The magnetic field data from THD are plotted too as a time reference. From top to bottom are the following: FGM data in the magnetopause local coordinate system; the electron energy spectrum from ESA instrument; the ion energy spectrum from SST and ESA; the ion density and temperature from ESA; and the thermal pressure (blue curve), the magnetic pressure (red curve), and the total pressure (black curve).

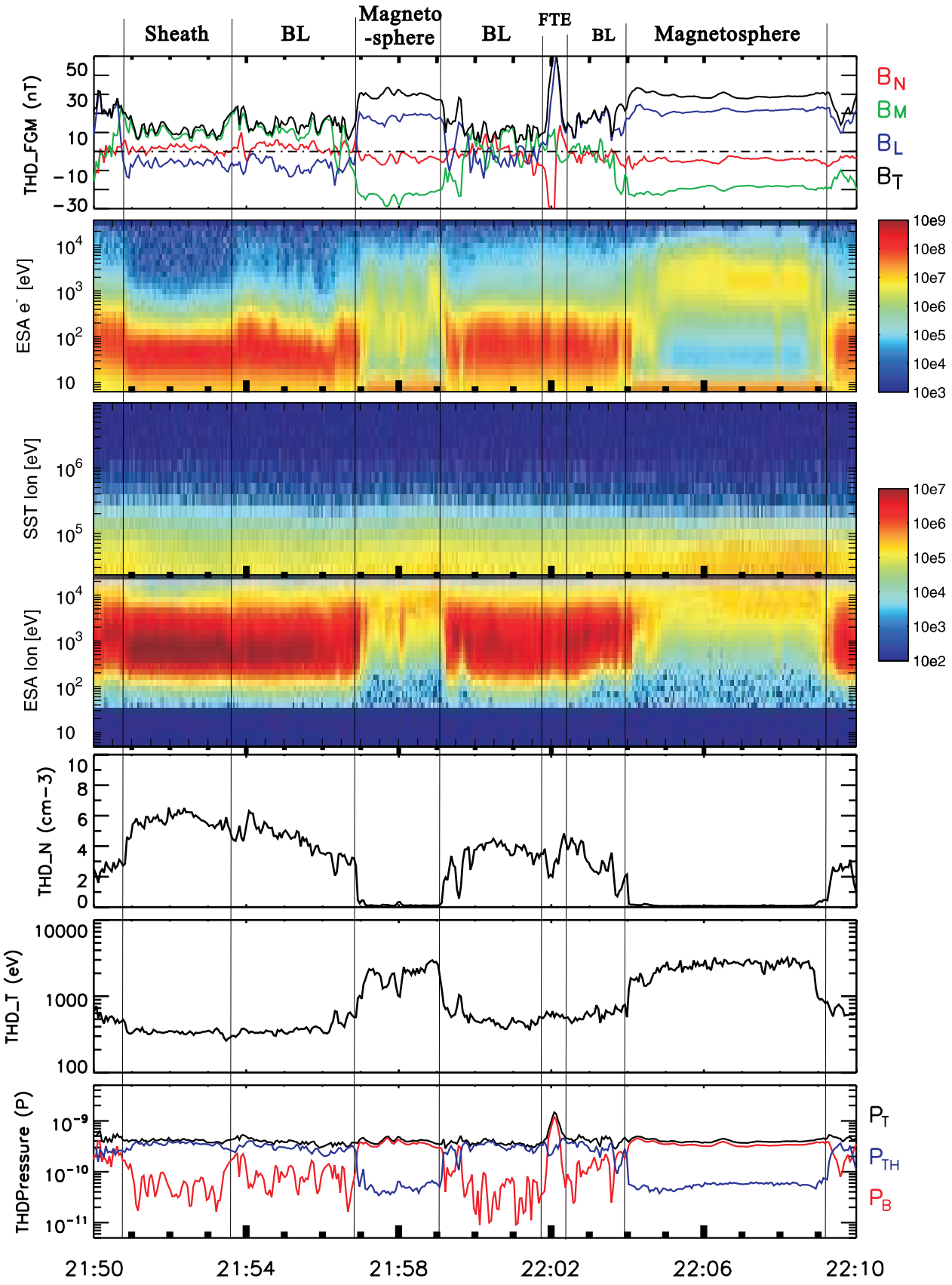
Sheath
BL
Magneto
-sphere
BL
FTE
BL
Magnetosphere
THD_FGM (nT)
50
30
10
−10
−30
B_N
B_M
B_L
B_T
ESA e⁻ [eV]
10^4
10^3
10^2
10
10e9
10e8
10e7
10e6
10e5
10e4
10e3
SST Ion [eV]
10^6
10^5
ESA Ion [eV]
10^4
10^3
10^2
10
10e7
10e6
10e5
10e4
10e3
10e2
THD_N (cm−3)
10
8
6
4
2
0
THD_T (eV)
10000
1000
100
THDPressure (P)
10^{-9}
10^{-10}
10^{-11}
P_T
P_{TH}
P_B
21:50
21:54
21:58
22:02
22:06
22:10

Figure 3

there might be a transition region between the FTE and the magnetosphere.

3.2. Plasma Observations

[15] The ESA and SST plasma data from THD are shown in Figure 3. The magnetic field data are plotted in the first panel for reference. The second panel displays the energy spectrum of the thermal electrons from ESA. There are three distinct regions with different electron energy ranges: from 10 eV to 200 eV (low energy), from 10 eV to 500 eV (midrange energy), and from 500 eV to 10 keV (high energy). The dense and low energy electrons (below 20 eV) are photoelectrons. The high-energy electrons were detected in the region we identified as the magnetosphere; both the low- and midrange-energy electrons, appeared in the region that we have identified as the magnetosheath only using magnetic field data. The electrons in the midrange energy are localized in the boundary layer (BL) between the magnetosphere and the sheath, and the magnitude of the magnetic field in this region differs from its values in the magnetosphere or in the sheath. The ion energy spectra from SST and ESA are displayed in the third and fourth panels. Typically, dense and low-energy ions (from $\sim$100 eV to $\sim$10 keV) detected by ESA can be clearly seen in the magnetosheath, and tenuous and high-energy ions (from $\sim$1 keV to 200 keV) measured by both ESA and SST appear during entries into the magnetosphere. Both low- and high-energy ions are present in the BL. During the encounter with the FTE around 2202 UT, the high-energy magnetospheric particles were not observed and the flux of ions and electrons measured by ESA instruments decreased slightly. The decreased density and the increased temperature inside the FTE led to an almost constant thermal pressure within the FTE (see the blue curve in the panel 7), while the magnetic pressure was significantly enhanced (the red curve of panel 7), and thus the total pressure was also enhanced significantly (the black curve). The β of the plasma (the ratio of the thermal pressure to the magnetic pressure) varied from $\sim$2 to $\sim$10 in the BL, while in the center of the FTE β dropped as low as 0.2 (not shown). The plasma and the magnetic field data suggest that the FTE was embedded in the BL which we henceforth identify as a region with the characteristic electron energy of 500 eV.

[16] The data from THE and THA were sufficiently similar that we show only the data from THE in Figure 4. Before flying by the FTE, THE was located in the magnetosheath and observed low-energy electrons (below 200 eV). As it approached the FTE (about 2202 UT), ESA registered an energy jump in electrons from 200 eV up to 500 eV indicating that THE entered the BL region; simultaneously the ion energy also increased slightly. A small increase in the temperature led to a small enhancement of the thermal pressure at about 2202 UT seen in panels 6 and 7 in Figure 4, and, during the pass by the FTE, the total pressure increased too. β in the BL region at THE was about 2 (not shown).

[17] THB and THC were the two satellites inside THD. The plasma profiles at these two satellites are also similar to each other and in this paper only the data from THB is shown in Figure 5. The plasma data of Figure 5 shows that THB moved between the magnetosphere and the BL. The FTE signature was detected by THB during its second entrance into the BL. The value of β in the dips of B_T which we have interpreted as encounters with a transition region between the magnetosphere and the FTE, was $\sim$2, similar to values in the BL detected by THA and THE just outside of the FTE. We believe that this indicates that the transition region was actually the BL region between the FTE and the magnetosphere.

3.3. FTE Motion

[18] Figure 6 displays the velocity of ions detected by the ESA instruments of the five THEMIS satellites and the FGM data from THD in the LMN coordinate system defined in section 3.1. When THD entered the BL, it observed high-speed flows with the dominant component in the $\vec{M}$ direction. The maximum observed velocity was $\sim$400 km/s at 2159:30 UT and after 2203 UT, respectively. The average velocity of the ions inside the FTE was $\sim$170 km/s and the FTE was located at the leading edge of the second velocity peak. When THC and THB encountered the FTE they recorded average velocities of $\sim$200 km/s mainly in the $\vec{M}$ direction; the velocity increased to as much as 300 km/s just outside of the FTE when the spacecraft encountered the BL region between the magnetosphere and the FTE. At THE and THA, through most of the period of Figure 6 there were flows of $\sim$230 km/s, but when THE and THA passed by the FTE, the flows slowed to $\sim$180 km/s before increasing slightly to about 200 km/s. We notice that the flows inside the FTE were slower than the ambient flows in the BL and thus that the FTE was an obstacle to the ambient BL flows.

[19] It is sometimes useful to analyze boundary structures in a deHoffmann-Teller (HT) frame [*deHoffmann and Teller*, 1950], a Galilean frame of reference in which the electric field perpendicular to the magnetic field vanishes. If this frame of reference exists, the observed magnetic structure is in a steady state [*Sonnerup et al.*, 1987, 1990]. We look for an HT frame using the observations at THD, THC and THB from 2201:30 UT to 2202:30 UT, from 2201:59 UT to 2202:20 UT, and from 2202:03 UT to 2202:16 UT, respectively. The scatterplot of the HT electric field $\vec{E}_{HT} = -\vec{V}_{HT} \times \vec{B}_o$ and the electric field inferred by $\vec{E}_o = -\vec{V}_o \times \vec{B}_o$ are shown in Figure 7, here the subscript o denotes the observations. The correlation coefficient between $\vec{E}_{HT}$ and $\vec{E}_o$ is 0.9791; the close correlation confirms that we can identify an HT frame for this event and in this frame the FTE structure was steady over time. The velocity of the frame, $\vec{V}_{HT}$, was ($-$105, 133, 20) km/s in GSM. In other words, in the observational frame, the steady FTE moved at this constant speed. The correlation coefficient further suggests that the FTE structure was not accelerating or decelerating significantly. In addition, the FTE was moving faster than the satellites whose speed was 1.0 km/s.

4. Fit to the KK95 Flux Rope Model

[20] With multiple measurements through and around the FTE, it is useful to fit the measurements to a model. We select the KK95 model, which allows for a finite contribution from thermal pressure gradients and thus does not require that the structure be force-free. The model was developed to describe flux ropes embedded in a neutral sheet as representative of conditions in the magnetotail. The

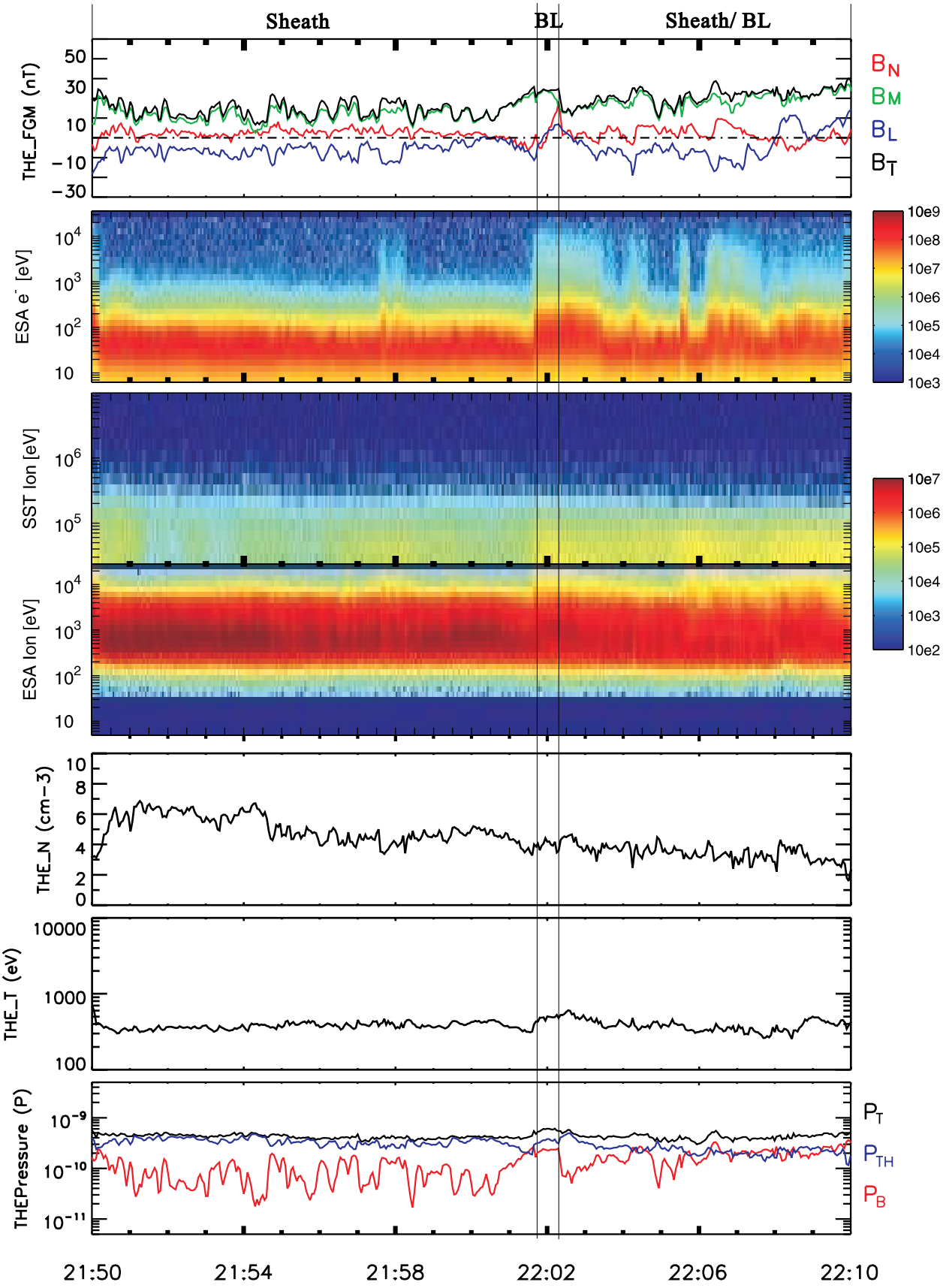

Figure 4. The plasma observations at THE. The format is the same as that of Figure 3.

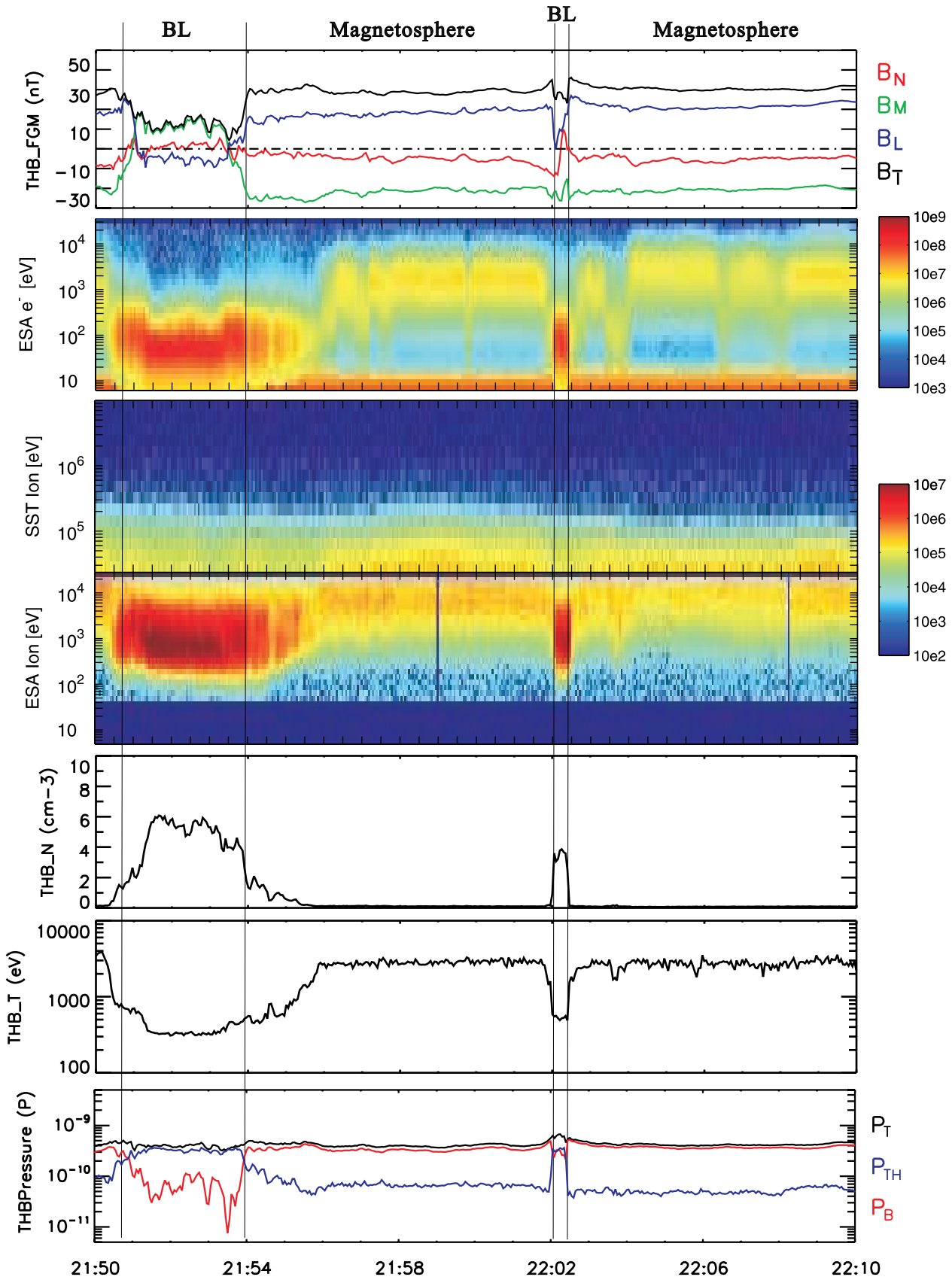

Figure 5. The plasma observations at THB. The format is the same as that of Figure 3.

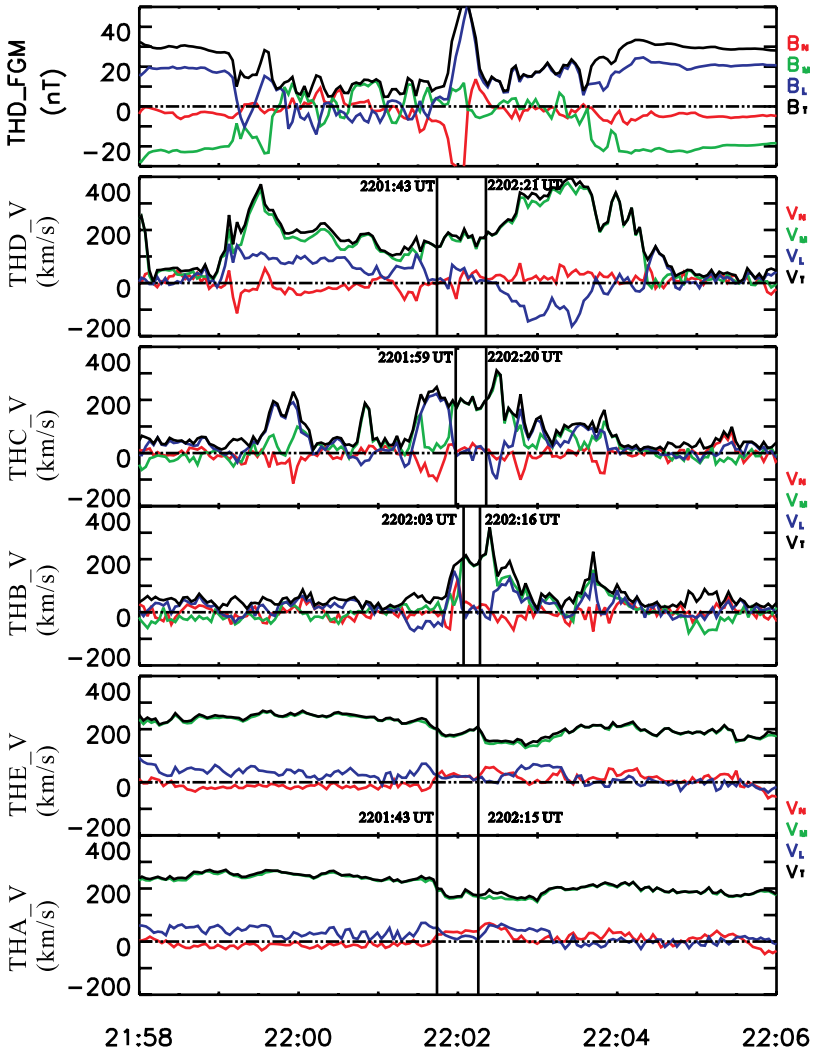

Figure 6. The ion velocity from ESA instruments. The magnetic field data from THD are plotted in the first panel as a time reference. From the second panel to bottom are the velocities observations from THD, THC, THB, THE, and THA. The vertical lines mark the time interval of the FTE, and they are the same as shown in Figure 2.

model can apply to a periodic array of flux ropes, but also can be linked to a Harris neutral sheet field at the boundary of a single unit of the periodic array, and that is the form that we adopt. The model describes the field and plasma pressure within the flux rope and in its perturbed surroundings.

4.1. Applicability of KK95 Model

[21] The flux rope that we seek to model here is embedded in BL where conditions closely approximate those applicable in the magnetotail neutral sheet. The magnetic field and plasma data shown in the Figures 2, 3, 4, 5, and 6 indicate that there were three distinct plasma regimes near the magnetopause: the magnetosphere, the magnetosheath and the BL between them. The FTE was fully embedded in the BL region. THE (see Figure 4) flew by the FTE in the BL region near the sheath as evident from the midrange-electron intensity; THB (Figure 5) grazed or flew by the FTE flank near the magnetosphere, but before and after encountering the FTE, THB briefly encountered the BL

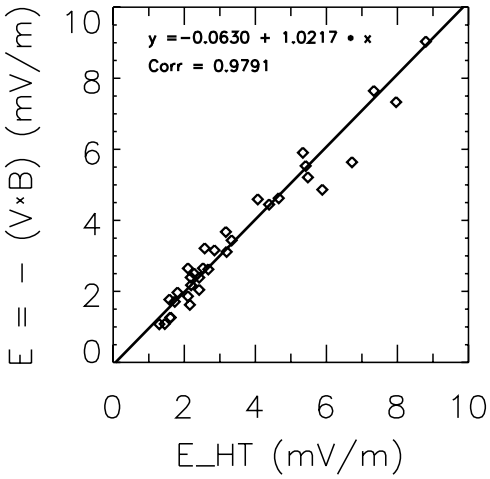

Figure 7. The scatterplot for the HT electric field $\vec{E}_{HT} = -\vec{V}_{HT} \times \vec{B}_o$ and the observational electric field inferred by $\vec{E}_o = -\vec{V}_o \times \vec{B}_o$.

Table 1. Typical Properties of the Plasma and the Magnetic Field in Different Regions of the BL

	Region		
Parameter	BL Between Magnetosheath and FTE (THE)	Near Center of BL (THD)	BL Between Magnetosphere and FTE (THB)
B_T(nT)	25	10–20	25
Dominant field component	$+B_M$	disturbed	$-B_M$
Electron energy range (eV)	10–500	10–500	10–500
β	~2	2–10	~2
Velocity (km/s)	~200	~400	~300

region; THD (Figure 3) crossed the FTE near its center, but both before and after encountering the FTE was located in the BL region. The parameters in different regions of BL encountered by these spacecraft are listed in Table 1. In the BL regions beside the FTE, the plasma parameters and the magnitude of the field are almost the same on the magnetospheric and magnetosheath sides, and the B_M components dominate but reverse sign. In the center of the BL β is much higher than elsewhere (THD). The BL seemed to be a current sheet [*Sibeck et al.*, 2008] with sheared magnetic field and these conditions are comparable with those near the current sheet in the tail, which suggests that the KK95 model provides a suitable approximation for fitting this event and is likely superior to other available models that do not include the properties of the field and plasma external to the flux rope. The properties of the BL may be associated with the formation of the FTE. We return to a discussion of this point later in the paper.

4.2. KK95 Flux Rope Model

[22] The internal features of a quasi-static magnetic structure are typically controlled by equation (1):

$$d\vec{V}/dt \equiv -\nabla P + \vec{J}\times\vec{B} = -\nabla P - \nabla B^2/2\mu_0 + (\vec{B}\cdot\nabla)\vec{B}/\mu_0 \quad (1)$$

where $-\nabla P$ is the thermal pressure gradient force, and $\vec{J}\times\vec{B}$ is the magnetic force. The latter can be decomposed into two terms: the "magnetic pressure gradient" force $-\nabla B^2/2\mu_0$ and the "magnetic tension" force $(\vec{B}\cdot\nabla)\vec{B}/\mu_0$. When $-\nabla P$ and $\vec{J}\times\vec{B}$ vanish separately, the magnetic structure is referred to as a "force-free" structure. We can estimate the individual force terms along the trajectory of THD; the inertial term $d\vec{V}/dt$ is found to be about 3×10^{-18} N/m^3, the thermal pressure gradient force is about 6×10^{-17} N/m^3, while the magnetic pressure gradient force is 4×10^{-16} N/m^3 which is much greater than the other two terms. Thus, the magnetic pressure gradient inside the FTE must be mainly balanced by the magnetic tension force, that is to say, the FTE is well approximated as a force-free structure.

[23] In this paper, we adopt the force-free version of the KK95 model to fit the THEMIS magnetic field observations of the FTE event. The parameters of the two-dimensional elliptical KK95 flux rope model do not vary along the direction of the core field denoted by $\vec{x}_3$; $\vec{x}_1$ is perpendicular to the current sheet, and $\vec{x}_2$ is parallel to the current sheet. In this coordinate system, the structure of flux rope is expressed by equation (2):

$$-\nabla^2 A_3 = (B_{2,\infty}/L)\exp(2A_3/B_{2,\infty}L) \quad (2)$$

with

$$A_3 = -B_{2,\infty}L\ln\chi \quad (3)$$

Here A_3 is the component of the vector potential in the $\vec{x}_3$ direction; $B_{2,\infty}$ is the asymptotic magnitude of the B_2 component far away from the center of the flux rope in the $\vec{x}_1$ direction ($x_1\rightarrow\pm\infty$); L is the scale length; and $\chi = (1+\varepsilon^2)^{1/2}\cosh(x_1/L) + \varepsilon\cos(x_2/L)$. ε controls the shape of the cross section of the flux rope: when $\varepsilon\rightarrow 0$, the solution of equation (2) reduces to a Harris neutral sheet; when ε increases, the cross section changes from an oblate to a circular shape.

[24] On the basis of the relation $\vec{B} = \nabla\times\vec{A}$, equation (3) gives the solutions for the magnetic field components in the $\vec{x}_1$ and $\vec{x}_2$ directions

$$[B_1,\ B_2,\ B_3] = \left[\frac{B_{2,\infty}}{\chi}\varepsilon\sin(x_2/L),\ \frac{B_{2,\infty}}{\chi}(1+\varepsilon^2)^{1/2}\sinh(x_1/L),\ B_3\right] \quad (4)$$

In the relevant force-free case, $\vec{J}\times\vec{B} = 0$, which implies that B_3 can be obtained from

$$B_3 = \frac{B_{2,\infty}}{\chi}\left(1+(B_{3,\infty}\chi/B_{2,\infty})^2\right)^{1/2} \quad (5)$$

where $B_{3,\infty}$ is the asymptotic magnitude of the B_3 component when $x_1\rightarrow\pm\infty$. This component allows for skewed asymptotic field lines. As pointed out by *Kivelson and Khurana* [1995], the solutions (4) and (5) describe a periodic array of flux ropes embedded in a Harris neutral sheet. In this paper we fit the FTE to one element of the flux rope array. Four free parameters, $B_{2,\infty}$, $B_{3,\infty}$, L and ε, are needed to constrain the geometry of a flux rope.

[25] As an example, Figure 8a shows a cross section of a flux rope modeled by the above solutions, in which $B_{2,\infty}$ = 20 nT, $B_{3,\infty}$ = 0 nT, and ε = 0.8. The cross section is quasi-elliptical. Hereafter in this paper, we refer to the coordinate system used in this analysis as the flux rope's local coordinate system.

4.3. Data Fitting

[26] The trajectory of a satellite relative to the FTE in this event approximates a straight line because the motion of the FTE is relatively quite fast and constant whereas the satellite is almost stationary. As evident from the blue line in Figure 8a, we need three parameters to describe the possible trajectories of a spacecraft relative to a flux rope: V, θ and D. V is the magnitude of the velocity of spacecraft relative to the flux rope. In a two-dimensional structure, the component of the relative velocity along the $\vec{x}_3$ direction is meaningless, so here V is, in fact, the velocity projected onto the cross section of flux rope. θ is the angle between $\vec{x}_1$ axis and the projected trajectory; it describes the direction of

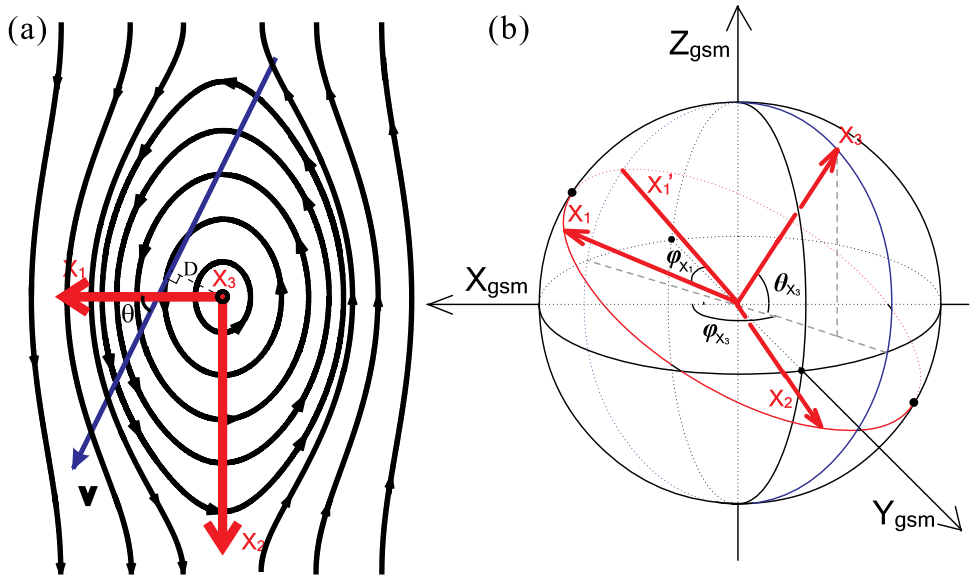

Figure 8. (a) Cross-sectional map of a flux rope described by KK95 force-free model. The blue straight line depicts the projection of a trajectory of spacecraft. (b) Three free parameters to control the relative orientations of a flux rope in the observational coordinate system, such as GSM.

the motion of a spacecraft relative to the cross section of the flux rope. D denotes the distance from the projected trajectory to the flux rope's center.

[27] The remaining step is to relate the unit vectors of the local FTE coordinate system to a physical coordinate system, such as GSM. Thus, we need three more parameters, θ_{X_3}, φ_{X_3} and φ_{X_1}, to control the possible relative orientations, as shown in Figure 8b. θ_{X_3} and φ_{X_3} are the latitude and the longitude of the $\vec{x}_3$ axis in the GSM coordinate system which constrain the direction of the $\vec{x}_3$ axis. The vector $\vec{x}'_1$ can be determined by $\vec{x}_3$ and Z_{GSM}, and in fact, $\vec{x}'_1$ is the intersection between the orthodrome perpendicular to $\vec{x}_3$ (the red curve on the surface of a sphere) and the orthodrome determined by Z_{GSM} and $\vec{x}_3$ (the blue one). Once $\vec{x}'_1$ is determined, the direction of the $\vec{x}_1$ axis can be readily specified by the azimuthal angle φ_{X_1} in the red orthodrome plane, and here $\vec{x}'_1$ is just taken as a reference direction.

[28] If we want to describe all the possible configurations of a flux rope and all the possible trajectories of a satellite relative to the flux rope, we must take all six free parameters, V, θ, D, θ_{X_3}, φ_{X_3} and φ_{X_1}, into account. Nevertheless, some free parameters can be constrained through the observations before carrying out a fitting. We have obtained the velocity of the FTE by the HT analysis, it was $\vec{V}_{HT} = (-105, 133, 20)$ km/s in GSM. For a given set of θ_{X_3}, φ_{X_3} and φ_{X_1}, the free parameters of V and θ can be obtained by projecting $\vec{V}_{HT}$ onto a cross-sectional plane of the flux rope determined by θ_{X_3}, φ_{X_3} and φ_{X_1}, thus we eliminate these two free parameters.

[29] There are four other free parameters, $B_{2,\infty}$, $B_{3,\infty}$, L and ε, which control the geometric structure of a flux rope. The magnetic field and plasma data indicate that THD was closest to the center of the FTE. THA and THE were located furthest from THD. By projecting the average FGM data of THA and THE between 2201:40 UT and 2202 UT onto the cross section, we obtained the estimation of the asymptotic value of B_2, that is, $B_{2,\infty}$. We take $B_{3,\infty}$, L and ε as free parameters. Thus a total of seven parameters must be determined. Relative distances between spacecraft are given in units of the scale length L, but knowledge of the spacecraft trajectories establishes the length scale.

[30] We fit the model by minimizing the parameter σ, the root mean square of the difference between the model and the observations. We refer to σ as the error estimator. Here

$$\sigma = \left\{ \left[\sum_{j=1}^{4} \sum_{n=1}^{N_j} \sum_{i=1}^{3} \left(B_{i,n}^{j,O} - B_{i,n}^{j,M} \right)^2 \right] \Big/ \left[3 \sum_{j=1}^{4} N_j \right] \right\}^{1/2} \quad (6)$$

where the superscripts O and M denote observation and model, respectively, j denotes the different spacecraft, N_j is the total number of the data points at each spacecraft, and i marks the different components of the magnetic field. In this paper, data from four spacecraft (THD, −C, −B and −E) are fitted to the model.

[31] The data between the vertical lines in each panel of Figure 2 are input into our fit (Data from THA are not included), and all these input data includes the FTE field or the BL field. The sheath and magnetospheric field is excluded. We obtain a best fit with σ = 4.4 nT. The fit yields the parameters: $\theta_{X_3} = 64°$, $\varphi_{X_3} = 217°$ and $\varphi_{X_1} = 8°$. Correspondingly, in GSM, the core field direction $\vec{x}_3$ is along (−0.350, −0.264, 0.899), the minor axis $\vec{x}_1$ lies along (0.627, 0.647, 0.434), and the major axis $\vec{x}_2$ is in the direction of (−0.696, 0.716, −0.061). At each spacecraft, three components and the total magnitude of the observed and the modeled magnetic field are shown in Figure 9 in the flux rope's local coordinate system. Although the magnetic components are reasonably well reproduced by the model (with a correlation coefficient of 0.9698), the B_1 components (the red curves) are less well represented than the other components, especially on the trailing edge of the flux rope at THC, −B, and −E. In Figure 10, the modeled (red

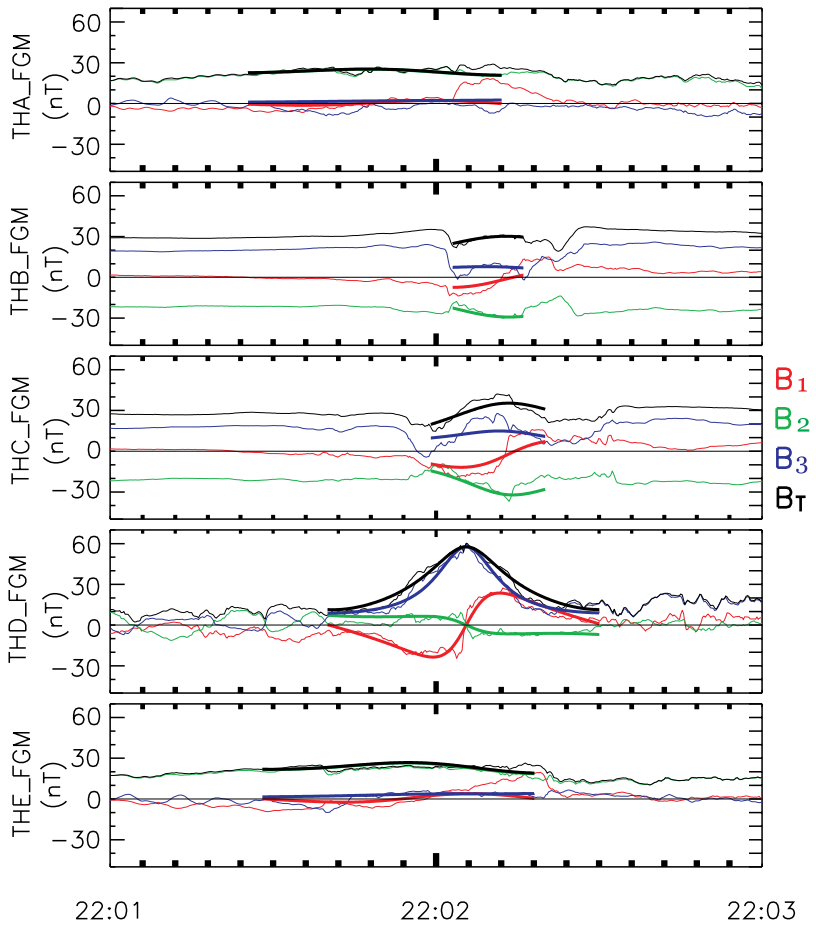

Figure 9. The observations and the modeled magnetic field in the flux rope's local coordinate system. From top to bottom, the data from all five spacecraft are displayed, and the different colors denote the different components (red, B_1; green, B_2; blue, B_3; black, B_T). The bold short curves represent the data from the model, and the thin curves represent the observations.

arrows) and observed (black arrows) magnetic field vectors are projected into the cross-sectional plane, and obviously on the trailing edge of the flux rope the observed magnetic field flares more than the modeled field.

[32] The parameters that control the internal structure of the flux rope are also obtained. $B_{2,\infty}$ is 24 nT, L is 1300 km and ε is 1.0. $B_{3,\infty}$ is found to be zero and it indicates that at large values of x_1 the magnetic field was dominantly perpendicular to the FTE's axis. The flux rope velocity perpendicular to its core field can be expressed as V and θ with $V = 170$ km/s and $\theta = 260°$. The velocity along the core field direction is 14 km/s. D represents the distance of the trajectory of THD from the center of the flux rope. THD crossed very close to the center of the flux rope and in our fit we obtain $D = 0$. The projected trajectories of the satellites onto the cross section are known through V, θ and D.

[33] We have also modeled the flux rope using an alternative approach in which we take V and θ as "free parameters," instead of using the HT approach above. All the parameters obtained from the two different approaches are listed in Table 2. The only parameters that change significantly are V (from 170 to 230 km/s) and L (from 1300 to 1600 km), while the error estimator, σ, changes little (from 4.4 nT to 3.9 nT). The comparison forces us to question which values of V and L better represent the actual features of the FTE. In order to determine why the values differ, we check the sensitivity of V to σ by setting V and L as free parameters. The results are shown in Figure 11. It is

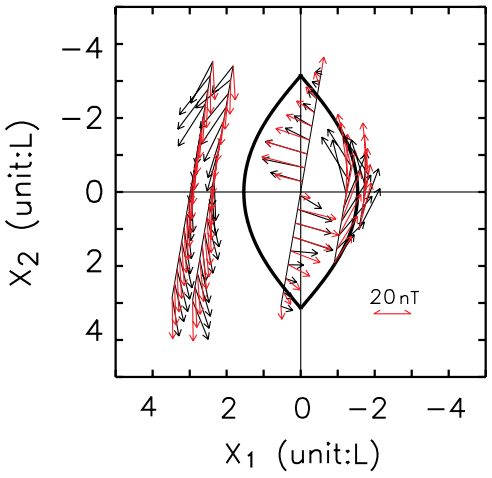

Figure 10. The modeled and observed magnetic field projected in the (x_1, x_2) plane: red for the model and black for the observations.

Table 2. Fitting Results From Two Approaches[a]

Condition for V and θ	σ (nT)	V (km/s)	θ (deg)	D (L)	θ_{X_s} (deg)	φ_{X_s} (deg)	φ_{X_n} (deg)	$B_{2,\infty}$ (nT)	L (km)	ε
Constrained by observations	4.4	170	260	0	64	217	8	24	1300	1
As free parameters	3.9	230	260	0	64	219	5	24	1600	1

[a]In one approach, V and θ are constrained by $\vec{V}_{HT}$; in the other one, V and θ are "free parameters."

evident that increasing V implies increasing L. However, V and L are not linearly related because a linear change of L changes the relative distance between a pair of spacecraft in units of L, and requires further modification of L to give the best fit. As V increases from 100 km/s to 300 km/s, σ initially decreases slightly, reaches its minimum at V = 225 km/s, and then increases with increasing V. When V changes by 25% (from 225 km/s to 170 km/s), σ changes by only 11% from 4.01 nT to 4.44 nT, which indicates that the fit is not sensitive to V over a plausible range of values. Thus it is reasonable to eliminate the free parameter V by using $\vec{V}_{HT}$ calculated from the observations. However, the direct fit also indicates that the deHoffmann-Teller analysis provides a velocity that represents the motion of the FTE with an error within 25%.

5. Discussion

5.1. Features Inside the FTE

[34] The correlation coefficient between the model and the data is close to 1. We believe that the correspondence between the magnetic field observations on five spacecraft and a simple model of flux rope supports the conclusion that the FTE observed has a helical internal structure. This conclusion that the FTE was a flux rope is consistent with the result of *Lui et al.* [2008] who reconstructed the FTE using the GS technique, although *Hasegawa et al.* [2007] caution that even an excellent fit of data to a flux rope model or the GS method does not necessarily prove the actual existence of such a flux rope. The existence of X lines both ahead of and behind the FTE, which we will discuss later, is also consistent with the conclusion that the FTE was a flux rope. There is also good evidence that the FTE was close to a force-free structure, both because the measured thermal pressure was constant across the flux rope and because a force-free magnetic model gives a satisfactory fit.

[35] On the basis of our fit, the spatial scale of the flux rope is about 3.1 × 6.3 L, that is, about 0.7 × 1.3 R_E (In a 2-D flux rope model, the length of the FTE cannot be inferred). The area of the cross section is 2.3 × 10^7 km^2. Our result differs considerably from the results of *Lui et al.* [2008] who reported scales less than 0.5 × 0.5 R_E for the same FTE that we analyze here. In their work, the outside boundary of the FTE was not clearly defined. Analyses of other dayside FTEs have found dimensions in the range we find here. *Saunders et al.* [1984] inferred that the cross section of the FTE they analyzed was also oblate and its typical scales were 1 × 2 R_E. The dimensions along the normal to the magnetopause of the flux ropes studied by *Hasegawa et al.* [2006] ranged from 2000 km to more than 1 R_E.

[36] For a force-free flux rope, the electrical current flows parallel (or antiparallel) to the magnetic field. From equa-

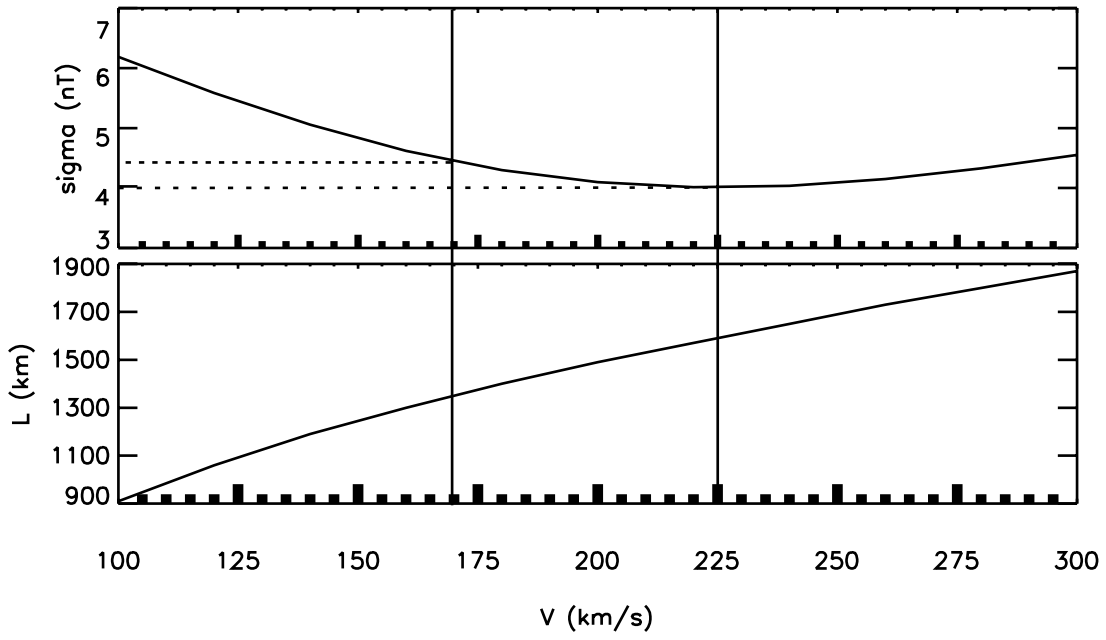

Figure 11. L and σ change with V. All other free parameters are fixed and are set the same as the condition with V constrained by V_{HT}.

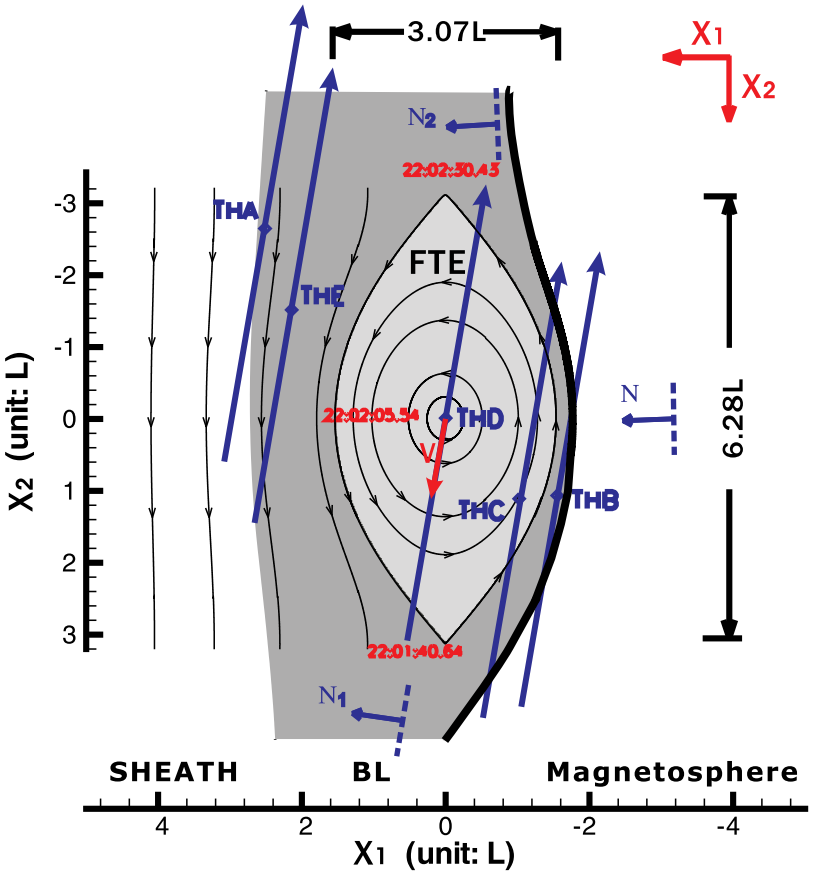

Figure 12. The modeled magnetic field inside and outside the FTE on 20 May 2007. The outmost closed line is the boundary of the FTE to its ambient BL field. The shaded region marks the BL between the magnetosphere and the sheath. The magnetosphere lies to the right of the bold black curve. The projection of the expected normal to the magnetopause is denoted by the vector $\vec{N}$. $\vec{N}_1$ and $\vec{N}_2$ denote the normal directions to the local magnetopause ahead of and behind the FTE, respectively. The straight blue lines show the projections of the trajectories of the five spacecraft on the cross-sectional plane. The red arrow in the center shows the motion of the flux rope perpendicular to its core field.

tion (2) we can express the current in terms of the magnetic field by

$$\vec{J} = \vec{B}/\left(\mu_0 \chi L\left(1 + \left(B_{3,\infty}\chi/B_{2,\infty}\right)^2\right)^{1/2}\right) \quad (7)$$

The current density reached a maximum of 100 nA/m^2 at the FTE's center. It is of interest to compare this with the magnetopause current density. The latter has been measured by the tetrahedral Cluster spacecraft constellation and typically ranges from ~9 nA/m^2 to ~40 nA/m^2, varying with magnetopause thickness [*Dunlop and Balogh*, 2005]. It is clear that FTE is a strong local current system on the magnetopause. The total current inside the FTE $I = \iint_{cross-section} J_Z ds$ reaches 0.3 MA, which is consistent with the result obtained by *Saunders et al.* [1984] and *Hasegawa et al.* [2006]. In this event, the amplitude of the sheared components of the sheath field and the magnetospheric field is about 30 nT, which corresponds to a local magnetopause current of about 0.3 MA/R$_E$. That is to say, although the current distributed unevenly, the total current inside the FTE was comparable with the current flowing within the same scale on the magnetopause (1.3 R$_E$ with current of ~0.4 MA on the magnetopause). The total magnetic flux through the cross section $\Theta = \iint_{cross-section} B_Z ds$ in this event is about 4 × 10^5 Wb, which is roughly 10% of the flux proposed for the *Saunders et al.* [1984] event. It seems that *Saunders et al.* [1984] overestimated the total flux inside the FTE they had studied, because they roughly multiplied the maximum of the core field component by the area of a rectangle in which the cross section was constrained whereas the model enables us to account for the decrease of axial current with distance from the center of the FTE.

5.2. Relation of the FTE to the Magnetopause

[37] We summarize our analysis of the configuration of the flux rope and the paths of the five THEMIS spacecraft relative to it in Figure 12. Figure 12 presents the projection of the internal field inside the FTE, the ambient BL magnetic field (the shaded region) and the satellites trajectories in a cross section plane. The last closed line is the boundary between the FTE and the ambient BL field. The magnetosphere lies to the right of the bold black curve in

Table 3. Orientation of the Core Field of the FTE on 20 May 2007 Inferred Through Different Methods

Method	Spacecraft	Core Field Direction (GSM)	Angle Relative to $\vec{x}_3$ (deg)
KK95	THB, −C, −D and −E	$\vec{x}_3$: (−0.350, −0.264, 0.899)	0.0
PAA	THD	$\vec{m}$: (−0.260, −0.149, 0.954)	8.9
GS	THD	$\vec{z}$: (−0.424, −0.247, 0.871)	4.6

Figure 12. It is clear that the FTE structure did not cling to the magnetosphere but that a BL region separated them; that is to say, the FTE was fully embedded in the BL region. A simulation reported by *Sibeck et al.* [2008] on this event produces a BL region and reveals it to be a current layer. The straight blue lines depict the projected trajectories of spacecraft between 2201:40.64 UT and 2202:30.43 UT. The actual spacecraft trajectories were almost parallel to the cross section since the component of $\vec{V}_{HT}$ along the core field direction was much smaller than the 170 km/s perpendicular velocity. Relative to the plane of the THD crossing, THA and THE crossed in planes lying 1.56 L and 1.31 L below and THC and THB crossed 0.63 L and 0.87 L above. THA and THE did not enter the flux rope but remained in the BL region when they passed by the FTE, although they detected the external magnetic perturbation and enhancement of the total pressure (Figure 4). THD crossed through the center of the FTE and THC grazed its flank; before and after crossing the FTE these two spacecraft passed through the BL. THB was briefly located in the BL when it passed by the FTE, and both in the BL and in the magnetosphere THB detected the enhancement of the total pressure (Figure 5). The analysis reveals that the FTE distorted the magnetopause locally into the magnetosphere as shown in Figure 12 and the FTE was embedded in a cavity on the magnetopause. It should be pointed out that when spacecraft were located either in the sheath/BL (THA and THE) or in the magnetosphere (THB and THC), they all remotely sensed the enhancement of the total pressure (Figures 3, 4, and 5) and the magnetic field perturbations, which were the signatures of the traveling compressional region around FTE [*Farrugia et al.*, 1987; *Liu et al.*, 2008].

[38] The determination of the normal to the magnetopause is critical for understanding the relation of a FTE to the magnetopause. In the studied event, THEMIS spacecraft encountered the FTE on the duskside near-equator magnetopause. THD crossed the magnetopause twice just before and soon after encountering the FTE (from 2159:10 UT to 2159:17 UT and from 2203:35 UT to 2203:40 UT), respectively. The MVA technique was applied to the data for these two magnetopause crossings and gave two estimates of the outward normal to the magnetopause: (0.788, 0.586, 0.187) in GSM ahead of the FTE ($\vec{N}_1$ shown in Figure 12) and (0.659, 0.726, 0.196) behind it ($\vec{N}_2$ shown in Figure 12). The two estimates which differ by 11° are significantly distinct and consistent with the suggestions that the FTE displaced the magnetopause locally into the magnetosphere. The normal direction, (0.692, 0.715, 0.092) in GSM, determined from the empirical model of *Shue et al.* [1998] and *Wang et al.* [2005] lies between the two normal directions determined by MVA technique, and appears to provide a good estimate of the outward magnetopause normal because the components of velocity and magnetic field along this direction were small compared with their tangential components along the magnetopause (Figures 2 and 6).

[39] The orientation of the axis of the flux rope, $\vec{x}_3$, obtained in our analysis, is along (−0.350, −0.264, 0.899) in GSM. This result is compared with results obtained from the PAA analysis and the GS technique listed in Table 3. The PAA analysis of the magnetic field data of THD between 2201:50 UT and 2202:20 UT gives a core field direction within 8.9° of our model result which deviates by only 4.6° from the core direction obtained with the GS technique [*Lui et al.*, 2008].

[40] Given the close correspondence among the different ways of estimating the core field direction and the magnetopause normal direction, it seems appropriate to ask whether the FTE orientation is aligned with the local magnetopause. We find that the scalar product of $\vec{x}_3$ and $\vec{N}$ is about −0.35 implying an angle of 110°. This nonzero scalar product would indicate that the south end of the flux rope was inclined into the sheath with an obliquity of about 20°, an obliquity that would not vanish over the range of inferred magnetopause normals. The pitch angles of the sheath ions inside the FTE were predominantly less than 90° (not shown), consistent with flow from the magnetosheath toward the magnetosphere and implying that the field lines at the southern end of the FTE were connected to the magnetosheath and that they connected to the magnetosphere at the northern end. If the southern end of the FTE was embedded in the magnetosheath, magnetosheath flow could plausibly twist the flux rope axis, explaining why the FTE was not purely parallel to the magnetopause.

5.3. Possible Origin

[41] The plasma flow and the magnetic field around the FTE provide clues for understanding its origin. Figure 13 gives the distributions of $V - V_{HT}$ and the magnetic field in the ($\vec{x}_1$, $\vec{x}_2$) plane along the trajectories of the five spacecraft. All five spacecraft were moving from the left bottom to the right. Data from THA, THE and THD are all from 2159 UT to 2204 UT, and data from THC and THB are given between 2201:59 UT and 2202:20 UT and between 2202:03 UT and 2202:16 UT, respectively. In these time intervals, all of the spacecraft were in the BL region or in the magnetosheath or experiencing an encounter with the FTE; data in the magnetosphere are excluded. The quasi-ellipses in the center of the two plots mark the outer boundary of the FTE. The projection of the normal to the magnetopause is indicated by blue arrows in each plot of Figure 13 and the bold red arrows mark the dominant vectors at their locations. Steady flows and a rather constant magnetic field in the sheath were detected by THA and THE before they entered into the BL. THD was initially in the BL region and observed a high-speed flow of about 170 km/s (in HT reference frame) dominantly in the $\vec{x}_2$ direction; the associated magnetic field was opposite to the sheath field

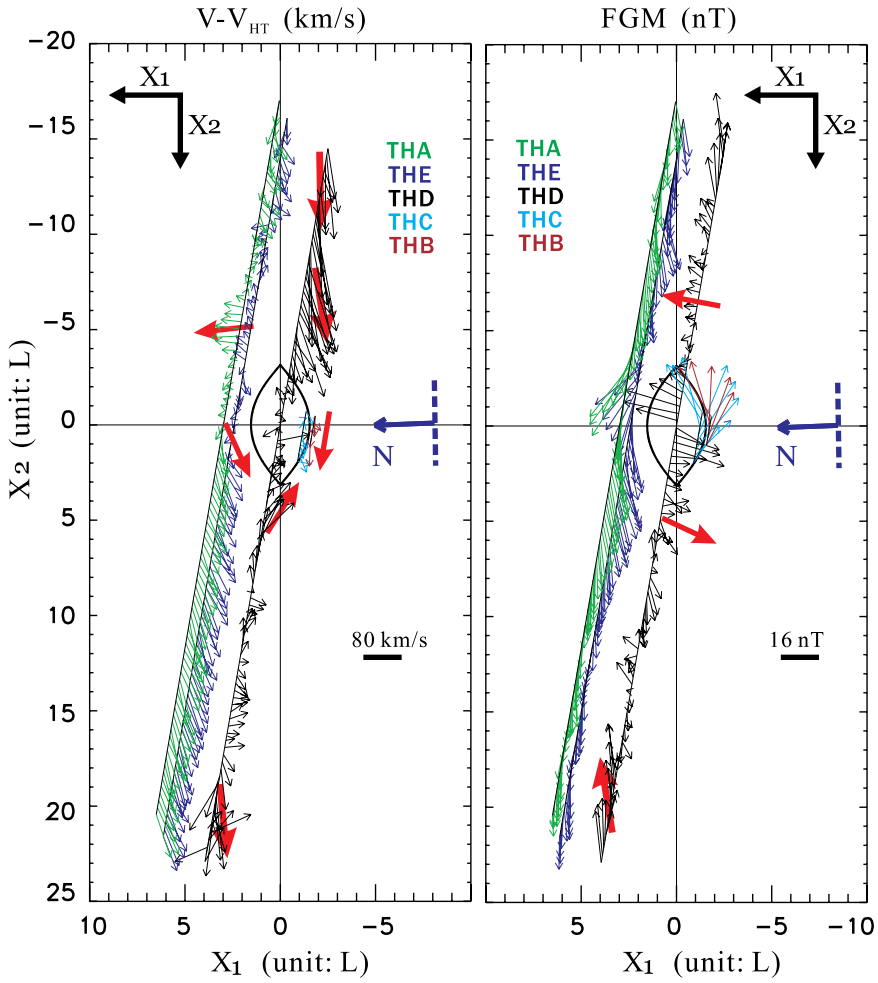

Figure 13. (left) The projection of $V - V_{HT}$ along the trajectories of the five spacecraft in the ($\vec{x}_1$, $\vec{x}_2$) plane. (right) The projection of the magnetic field along the trajectories of the five spacecraft in the ($\vec{x}_1$, $\vec{x}_2$) plane. N marks the projection of the normal to the magnetopause. Two X lines may exist ahead of and behind the flux rope, respectively.

recorded by the outermost satellites THA and THE. Just before THD entered the FTE, a high-speed convective flow mainly along $-\vec{x}_2$ was observed. These two opposed flows and their associated magnetic field were different from those in the sheath and suggest that there was an X line ahead of the FTE.

[42] Another X line following the FTE can be also inferred from the distribution of flows and magnetic field. After traversing the FTE, THD encountered a strong flow with a speed of over 200 km/s in HT reference frame. This flow was also convective with its dominant component along $\vec{x}_2$ and the dominant magnetic field in the $\vec{x}_3$ and $\vec{x}_1$ direction. The residue of the fast flow after subtracting the magnetosheath background flow was about 170 km/s, which was comparable with but a little bit slower than the local Alfvén speed (B: ~20 nT, N_i: ~4/cm^{-3} and V_A: ~210 km/s), suggesting that there was another X line behind this flow. The flow from this X line was much faster than those from the first X line (Figure 13), indicating that this X line was still active while the first one may have been less active or fossil. The two X lines ahead of and behind the FTE, respectively, would be consistent with the view that the flux-rope-type FTE was produced by reconnection at two X lines.

[43] The configurations of the sheath and magnetospheric field around the reconnection site are critical for understanding how reconnection generated the flux-rope-type FTE. High-energy magnetospheric particles are absent within the FTE, which suggests that the FTE was not currently formed but had existed long enough for the high-energy particles to escape along the opened magnetic field lines inside the FTE, but we have no way to determine where and when the FTE was generated. Thus the field configuration at the reconnection site cannot be obtained directly from the observations. Nevertheless, the fact that the two X lines were still active just ahead of and behind the FTE suggests that the FTE was observed not very long after or very far from when and where it formed. Therefore we will simply assume that the sheath and magnetospheric field configurations at the reconnection sites did not differ significantly from those around the observed FTE. The sheath field was ~20 nT (THA in Figure 9), dominantly in the $+\vec{x}_2$ direction, and the magnetospheric field was about (0, −20, 20) nT (THB in Figure 9); that is, they were not

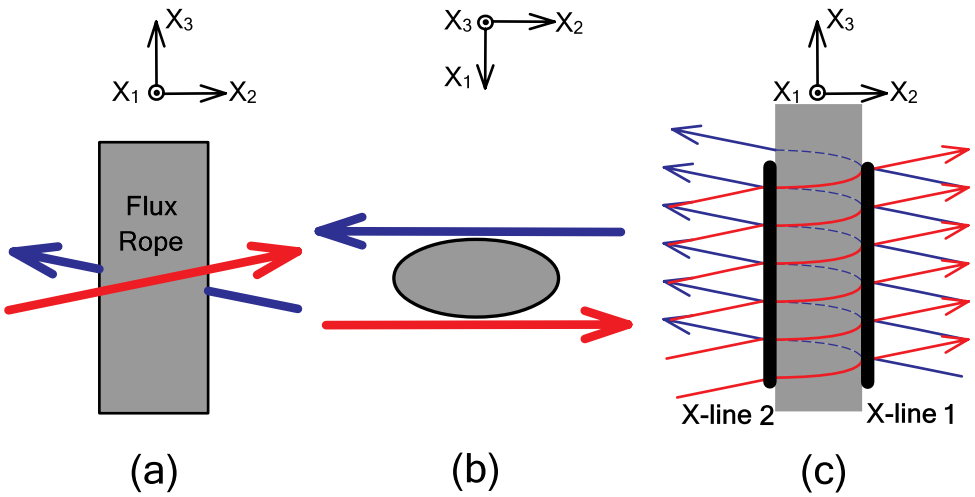

Figure 14. Schematics representing the formation of the FTE on the magnetopause. (a) The magnetic field beside the FTE, viewed toward the $-\vec{x}_1$ direction. (b) The magnetic field beside the FTE viewed toward the $-\vec{x}_3$ direction. (c) The generation of the FTE by component reconnection at two X lines. The FTE moved approximately along $\vec{x}_2$; X line 1 was ahead of the FTE, and X line 2 was behind. If the two X lines formed synchronously, the red and blue lines represent the magnetospheric and the sheath field, respectively. If X line 1 formed first, the red and the blue lines still represent the sheath and the magnetospheric field lines; when reconnection took place later on X line 2, the red and blue lines should be thought of as the sheared field lines recently reconnected on X line 1. If X line 2 remained active, the reconnection on this X line would finally have involved the sheath and the magnetospheric field.

strictly antiparallel and component reconnection must have occurred. We also notice that the BL field on the two sides of the FTE was ~25 nT, but the dominant components in the $\vec{x}_2$ direction were oppositely oriented on the magnetosphere and magnetosheath sides of the FTE (THE, −B and −C in Figure 9). In such magnetic field configurations, two X lines could form through reconnection of fields in the magnetosphere and the magnetosheath and/or roughly antiparallel fields inside the BL.

[44] How might the two X lines have created an FTE? Figure 14 schematically shows the field configurations (the red and blue arrows denote the magnetosheath and the magnetosphere field, respectively) and the two X lines (X line 1 is ahead of the FTE and X line 2 is the following one) around the FTE. If the two X lines formed at the same time, the relevant magnetosheath or magnetosphere field lines would reconnect twice synchronously on the two X lines and thus form a twisted and rope-like structure between them [*Lee and Fu*, 1985]; on the other hand, if X line 1 formed first among the sheath and magnetosphere field lines, the subsequent reconnection on X line 2 would have occurred initially among the oppositely oriented field lines recently reconnected on X line 1 and thus have formed a flux rope [*Raeder*, 2006; *Hughes and Sibeck*, 1987]. In this case, reconnection may ultimately have involved the magnetosheath and magnetosphere field lines. As mentioned above, when the FTE was encountered, X line 1 was not very active or possibly fossil while X line 2 was still active, suggesting that after the formation of FTE, reconnection continued among the magnetosheath and magnetosphere field lines on the still-active X line 2, and that the recently reconnected field lines and the heated particles generated through reconnection may have formed a so-called BL region around the FTE.

[45] The FTE was thus embedded in the BL region. In this case, it should have convected away with the high-speed flow ejected from X line 2 along $\vec{x}_2$. However, our observations indicate that the motion of the FTE was slower than this high-speed flow and even slower than the background sheath flow. Before and during the formation of the FTE, the high-speed flow along $-x_2$ from the active X line 1 may have decelerated the x_2 oriented background sheath flow and thus generated a slowly moving FTE; at the time of FTE encounter, the high-speed flow from the still-active X line 2 seems not to have accelerated the FTE significantly [*Raeder*, 2006]. In addition, field lines passing through the FTE and connecting to the magnetosphere at the FTE's ends may also impede the motion of the FTE [*Fu et al.*, 1990]. This scenario has been used to interpret slowing of flux ropes in the magnetotail before their release [*Hughes and Sibeck*, 1987].

[46] The interactions between the slowly moving FTE and the high-speed flow behind it modified both of them. The high-speed flows were diverted by the relatively incompressible obstacle [*Farrugia et al.*, 1987] and the effect is clearly seen behind and beside the FTE in Figure 13. The interaction also affected the internal and ambient field of the FTE, and on the trailing edge of the FTE, the modeled B_1 component deviated considerably from the observed field (see Figures 9 and 10), which was the greatest source of error of fit.

6. Summary and Conclusions

[47] An FTE was encountered by all five THEMIS spacecraft outside the dusk magnetopause on 20 May 2007. Because the thermal pressure was nearly constant across the structure, we were able to fit the magnetic

observations to a force-free flux rope model. Although interactions between the FTE and the ambient flows slightly modify the force-free condition, the high correlation coefficient of the model and the observations indicates that this FTE deviated only slightly from the force-free condition. From the fit, we were able to obtain the critical geometric parameters of this FTE, including the orientation of the core field, the shape and the dimensions of its cross section. We also calculated the electric current and the total magnetic flux inside the FTE. Magnetic field data and plasma data show that this FTE was fully embedded in the boundary region between the magnetosheath and the magnetosphere. The magnetic configuration and the flows around the FTE suggest that component reconnection at two X lines, as proposed by *Lee and Fu* [1985] and *Raeder* [2006], provides a satisfactory candidate mechanism for the generation of this FTE, although we cannot determine whether the two X lines formed synchronously. The presence of the two X lines and the ongoing reconnection after the formation of the FTE seems not consistent with the transient and patchy reconnection model of *Russell and Elphic* [1978]. Both the satisfactory fit and the existence of two X lines imply that the FTE had a helical internal structure, that is, the FTE was a flux rope. We have not been able to find a way in which the *Scholer* [1988] and *Southwood et al.* [1988] model of an FTE would produce a flux rope.

[48] **Acknowledgments.** This work is supported by NASA's THEMIS project under contract NAS5-02099. The authors acknowledge K. H. Glassmeier, U. Auster, and W. Baumjohann for the use of FGM data provided under the lead of the Technical University of Braunschweig and with financial support through the German Ministry for Economy and Technology and the German Center for Aviation and Space (DLR) under contract 50 OC 0302D. Thanks are also given to D. Larson and R. P. Lin for use of SST data and to C. W. Carlson and J. P. McFadden for use of ESA data.

[49] Wolfgang Baumjohann thanks Vladimir Semwnovich Semenov and another reviewer for their assistance in evaluating this paper.

References

Angelopoulos, V. (2008), The THEMIS mission, *Space Sci. Rev.*, doi:10.1007/s11214-008-9336-1, in press.

Auster, H. U., et al. (2008), The THEMIS Fluxgate Magnetometer, *Space Sci. Rev.*, doi:10.1007/s11214-008-9365-9, in press.

Berchem, J., and C. T. Russell (1984), Flux transfer events on the magnetopause: Spatial distribution and controlling factors, *J. Geophys. Res.*, *89*, 6689–6703, doi:10.1029/JA089iA08p06689.

Cowley, S. W. H. (1976), Comments on the merging of nonantiparallel magnetic fields, *J. Geophys. Res.*, *81*, 3455–3458, doi:10.1029/JA081i019p03455.

Crooker, N. U. (1979), Dayside merging and cusp geometry, *J. Geophys. Res.*, *84*, 951–959, doi:10.1029/JA084iA03p00951.

Daly, P. W., E. Keppler, D. J. Williams, and C. T. Russell (1981), Particle signature of magnetic flux transfer events at the magnetopause, *J. Geophys. Res.*, *86*, 1628–1632, doi:10.1029/JA086iA03p01628.

Daly, P. W., R. P. Rijnbeek, N. Sckopke, C. T. Russell, and M. A. Saunders (1984), The distribution of reconnection geometry in flux transfer events using energetic ion, plasma and magnetic data, *J. Geophys. Res.*, *89*, 3843–3854, doi:10.1029/JA089iA06p03843.

deHoffmann, F., and E. Teller (1950), Magneto-hydrodynamic shocks, *Phys. Rev.*, *80*, 692–703, doi:10.1103/PhysRev.80.692.

Dungey, J. W. (1961), Interplanetary magnetic field and the auroral zones, *Phys. Rev. Lett.*, *6*, 47–48, doi:10.1103/PhysRevLett.6.47.

Dunlop, M. W., and A. Balogh (2005), Magnetopause current as seen by Cluster, *Ann. Geophys.*, *23*, 901–907.

Elphic, R. C., and C. T. Russell (1983), Magnetic flux ropes in the Venus ionosphere: Observations and models, *J. Geophys. Res.*, *88*, 58, doi:10.1029/JA088iA01p00058.

Elphic, R. C., C. T. Russell, J. A. Slavin, and L. H. Brace (1980), Observations of the dayside ionopause and ionosphere of Venus, *J. Geophys. Res.*, *85*, 7679, doi:10.1029/JA085iA13p07679.

Farrugia, C. J., et al. (1987), Field and flow perturbations outside the reconnected field line region in flux transfer events: Theory, *Planet. Space Sci.*, *35*(2), 227–240, doi:10.1016/0032-0633(87)90091-2.

Farrugia, C. J., D. J. Southwood, and S. W. H. Cowley (1988), Observations of flux transfer events, *Adv. Space Res.*, *8*(9–10), 249–258, doi:10.1016/0273-1177(88)90138-X.

Fu, Z. F., L. C. Lee, and Y. Shi (1990), A three-dimensional MHD simulation of the multiple X line reconnection process, in *Physics of Magnetic Flux Ropes*, *Geophys. Monogr. Ser.*, vol. 58, edited by C. T. Russell, E. R. Priest, and L. C. Lee, pp. 515–519, AGU, Washington, D. C.

Gonzalez, W. D., and F. S. Mozer (1974), A quantitative model for the potential resulting from reconnection with an arbitrary interplanetary magnetic field, *J. Geophys. Res.*, *79*, 4186–4194, doi:10.1029/JA079i028p04186.

Hasegawa, H., B. U. Sonnerup, C. J. Owen, B. Klecker, G. Paschmann, A. Balogh, and H. Reme (2006), The structure of flux transfer events recovered from Cluster data, *Ann. Geophys.*, *24*, 603–618.

Hasegawa, H., et al. (2007), Reconstruction of a bipolar magnetic signature in an earthward jet in the tail: Flux rope or 3D guide-field reconnection?, *J. Geophys. Res.*, *112*, A11206, doi:10.1029/2007JA012492.

Hughes, W., and D. Sibeck (1987), On the 3-dimensional structure of plasmoids, *Geophys. Res. Lett.*, *14*(6), 636–639, doi:10.1029/GL014i006p00636.

Kivelson, M. G., and K. K. Khurana (1995), Models of flux ropes embedded in a Harris neutral sheet: Force-free solutions in low and high beta plasmas, *J. Geophys. Res.*, *100*, 23,637–23,645, doi:10.1029/95JA01548.

Le, G., et al. (2008), Flux transfer events simultaneously observed by Polar and Cluster: Flux rope in the subsolar region and flux tube addition to the polar cusp, *J. Geophys. Res.*, *113*, A01205, doi:10.1029/2007JA012377.

Lee, L. C., and Z. F. Fu (1985), A theory of magnetic flux transfer at the Earth's magnetopause, *Geophys. Res. Lett.*, *12*, 105–108, doi:10.1029/GL012i002p00105.

Lemaire, J., M. J. Rycroft, and M. Roth (1979), Control of impulsive penetration of solar wind irregularities into the magnetosphere by the interplanetary magnetic field direction, *Planet. Space Sci.*, *27*, 47–57, doi:10.1016/0032-0633(79)90146-6.

Liu, Z. X., and Y. D. Hu (1988), Local magnetic reconnection caused by vortices in the flow field, *Geophys. Res. Lett.*, *15*, 752–755, doi:10.1029/GL015i008p00752.

Liu, J., V. Angelopoulos, D. Sibeck, T. Phan, Z. Y. Pu, J. McFadden, K. H. Glassmeier, and H. U. Auster (2008), THEMIS observations of the dayside traveling compression region and flows surrounding flux transfer events, *Geophys. Res. Lett.*, *35*, L17S07, doi:10.1029/2008GL033673.

Lui, A. T. Y., D. G. Sibeck, T. Phan, V. Angelopoulos, J. McFadden, C. Carlson, D. Larson, J. Bonnell, K.-H. Glassmeier, and S. Frey (2008), Reconstruction of a magnetic flux rope from THEMIS observations, *Geophys. Res. Lett.*, *35*, L17S05, doi:10.1029/2007GL032933.

Lundquist, S. (1950), Magnetohydrostatic field, *Ark. Fys.*, *2*, 361.

McFadden, J. P., et al. (2008), The THEMIS ESA plasma instrument and in-flight calibration, *Space Sci. Rev.*, doi:10.1007/s11214-008-9440-2, in press.

Moldwin, M. B., and W. J. Hughes (1991), Plasmoids as magnetic flux ropes, *J. Geophys. Res.*, *96*, 14,051, doi:10.1029/91JA01167.

Paschmann, G., G. Haerendel, I. Papamastorakis, N. Sckopke, S. J. Bame, J. T. Gosling, and C. T. Russell (1982), Plasma and magnetic field characteristics of magnetic flux transfer events, *J. Geophys. Res.*, *87*, 2159–2168, doi:10.1029/JA087iA04p02159.

Pu, Z. Y., P. T. Hou, and Z. X. Liu (1990), Vortex-induced tearing mode instability as a source of flux transfer events, *J. Geophys. Res.*, *95*, 18,861–18,869, doi:10.1029/JA095iA11p18861.

Pu, Z. Y., et al. (2005), Multiple flux rope events at the high-latitude magnetopause: Cluster/Rapid observation on 26 January, 2001, *Surv. Geophys.*, *26*, 193–214, doi:10.1007/s10712-005-1878-0.

Raeder, J. (2006), Flux transfer events: 1. Generation mechanism for strong southward IMF, *Ann. Geophys.*, *24*, 381–392.

Rijnbeek, R. P., S. W. H. Cowley, D. J. Southwood, and C. T. Russell (1984), A survey of dayside flux transfer events observed by ISEE 1 and 2 magnetometers, *J. Geophys. Res.*, *89*, 786–800, doi:10.1029/JA089iA02p00786.

Russell, C. T., and R. C. Elphic (1978), Initial ISEE magnetometer results—Magnetopause observations, *Space Sci. Rev.*, *22*, 681–715, doi:10.1007/BF00212619.

Sanny, J., D. G. Sibeck, C. C. Venturini, and C. T. Russell (1996), A statistical study of transient events in the outer dayside magnetosphere, *J. Geophys. Res.*, *101*, 4939–4952, doi:10.1029/95JA03063.

Saunders, M. A., C. T. Russell, and N. Sckopke (1984), Flux transfer events—Scale size and interior structure, *Geophys. Res. Lett.*, *11*, 131–134, doi:10.1029/GL011i002p00131.

Scholer, M. (1988), Magnetic flux transfer at the magnetopause based on single X line bursty reconnection, *Geophys. Res. Lett.*, *15*, 291–294, doi:10.1029/GL015i004p00291.

Shue, J.-H., et al. (1998), Magnetopause location under extreme solar wind conditions, *J. Geophys. Res.*, *103*, 17,691, doi:10.1029/98JA01103.

Sibeck, D. G., W. Baumjohann, R. C. Elphic, D. H. Fairfield, and J. F. Fennell (1989), The magnetospheric response to 8-minute period strong-amplitude upstream pressure variations, *J. Geophys. Res.*, *94*, 2505–2519, doi:10.1029/JA094iA03p02505.

Sibeck, D. G., M. Kuznetsova, V. Angelopoulos, K.-H. Glaßmeier, and J. P. McFadden (2008), Crater FTEs: Simulation results and THEMIS observations, *Geophys. Res. Lett.*, *35*, L17S06, doi:10.1029/2008GL033568.

Sonnerup, B. U. Ö., and L. J. Cahill Jr. (1967), Magnetopause structure and attitude from Explorer 12 observations, *J. Geophys. Res.*, *72*(1), 171–183.

Sonnerup, B. U. O., and M. Guo (1996), Magnetopause transects, *Geophys. Res. Lett.*, *23*, 3679–3682, doi:10.1029/96GL03573.

Sonnerup, B. U. O., I. Papamastorakis, G. Paschmann, and H. Lühr (1987), Magnetopause properties from AMPTE/IRM observations of the convection electric field: Method development, *J. Geophys. Res.*, *92*, 12,137, doi:10.1029/JA092iA11p12137.

Sonnerup, B. U. O., I. Papamastorakis, G. Paschmann, and H. Lühr (1990), The magnetopause for large magnetic shear: Analysis of convection electric fields from AMPTE/IRM, *J. Geophys. Res.*, *95*, 10,541, doi:10.1029/JA095iA07p10541.

Southwood, D. J., C. J. Farrugia, and M. A. Saunders (1988), What are flux transfer events?, *Planet. Space Sci.*, *36*, 503–508, doi:10.1016/0032-0633(88)90109-2.

Wang, Y., et al. (2005), Initial results of high-latitude magnetopause and low-latitude flank flux transfer events from 3 years of Cluster observations, *J. Geophys. Res.*, *110*, A11221, doi:10.1029/2005JA011150.

Wang, Y. L., R. C. Elphic, B. Lavraud, M. G. G. T. Taylor, J. Birn, C. T. Russell, J. Raeder, H. Kawano, and X. X. Zhang (2006), Dependence of flux transfer events on solar wind conditions from 3 years of Cluster observations, *J. Geophys. Res.*, *111*, A04224, doi:10.1029/2005JA011342.

Xiao, C. J., Z. Y. Pu, Z. W. Ma, S. Y. Fu, Z. Y. Huang, and Q. G. Zong (2004), Inferring of flux rope orientation with the minimum variance analysis technique, *J. Geophys. Res.*, *109*, A11218, doi:10.1029/2004JA010594.

Zhou, X.-Z., Q.-G. Zong, Z. Y. Pu, T. A. Fritz, M. W. Dunlop, Q. Q. Shi, J. Wang, and Y. Wei (2006), Multiple triangulation analysis: Another approach to determine the orientation of magnetic flux ropes, *Ann. Geophys.*, *24*, 1759–1765.

Zong, Q.-G., et al. (1997), Geotail observations of energetic ion species and magnetic field in plasmoid-like structure in the course of an isolated substorm event, *J. Geophys. Res.*, *102*, 11,409–11,428, doi:10.1029/97JA00076.

Zong, Q.-G., T. A. Fritz, H. Spence, M. Dunlop, Z. Y. Pu, A. Korth, P. W. Daly, A. Balogh, and H. Reme (2003), Bursty energetic electrons confined in flux ropes in the cusp region, *Planet. Space Sci.*, *51*, 821–830, doi:10.1016/S0032-0633(03)00116-8.

V. Angelopoulos, K. K. Khurana, M. G. Kivelson, J. Liu, H. Zhang, and X.-Z. Zhou, Institute of Geophysics and Planetary Physics, University of California, 6863 Slichter Hall, Los Angeles, CA 90095, USA. (hzhang@igpp.ucla.edu)

Z. Y. Pu, School of Earth and Space Sciences, Peking University, No. 5 Yiheyuan Street, Beijing 100871, China.

Q.-G. Zong, Center for Atmospheric Research, University of Massachusetts Lowell, 600 Suffolk Street, Lowell, MA 01854, USA.